Experiments and Simulations of Short-Pulse Laser-Pumped Extreme Ultraviolet Lasers

G. J. Tallents, Y. Abou-Ali, A. Demir, Q. Dong, M. H. Edwards, P. Mistry, and G. J. Pert

Invited Paper

Abstract—Recent experimental work on the development of extreme ultraviolet lasers undertaken using as the pumping source the VULCAN laser at the Rutherford Appleton Laboratory is compared to detailed simulations. It is shown that short duration (∼picosecond) pumping can produce X-ray laser pulses of a few picosecond duration and that measurement of the emission from the plasma can give an estimate of the duration of the gain coefficient. The Ehybrid fluid and atomic physics code developed at the University of York is used to simulate X-ray laser gain and plasma emission. Two postprocessors to the Ehybrid code are utilized: 1) to raytrace the X-ray laser beam amplification and refraction and 2) to calculate the radiation emission in the kiloelectronvolt photon energy range. The raytracing and spectral simulations are compared, respectively, to measured X-ray laser output and the output of two diagnostics recording transverse X-ray emission. The pumping laser energy absorbed in the plasma is examined by comparing the simulations to experimental results. It is shown that at high pumping irradiance ($> 10^{15}$ Wcm^{-2}), fast electrons are produced by parametric processes in the preformed long scale-length plasmas. These fast electrons do not pump the population inversion and so pumping efficiency is reduced at high irradiance.

Index Terms—Extreme ultraviolet (EUV), plasma, X-ray laser.

I. INTRODUCTION

PLASMA-BASED extreme ultraviolet (EUV) lasers (often referred to as X-ray lasers) have been investigated almost from the time of the invention of the laser. Measurement of definitive high-output lasing at wavelengths shorter than the ultraviolet was elusive despite many theoretical studies and some experiments [1] until the mid 1980s when conclusive evidence for an "X-ray laser" operating at a wavelength of 21 nm was produced [2]. This X-ray laser was created in a plasma produced by focusing into a line on a foil target the most energetic nanosecond duration infra-red laser then available (NOVA, Lawrence Livermore National Laboratory). The lasing action at 21 nm along the line was confirmed by measuring the variation of the spectral output as a function of the plasma length and from the observation that the output was highly anisotropic, in fact, a beam of 21-nm photons.

The shortest wavelength laser produced so far at 3.5 nm was similarly created using the NOVA near-infra-red laser incident onto a foil target [3]. The laser action occurs due to electron collisional pumping in the laser-produced plasma expanding away from the solid surface. Laser plasmas also have the record for the shortest wavelength-saturated laser at 5.9 nm [4]. This was achieved using the VULCAN laser at the Rutherford Appleton Laboratory with enhanced efficiency and a much smaller laser energy due to the use of a prepulse forming a preplasma into which the main pumping laser pulse interacts.

Saturation of a laser occurs when stimulated emission becomes a significant depletion process on the population of the upper quantum state. It is an important milestone as the laser output is close to maximum for the experimental configuration, and additionally the shot-to-shot variation and beam profile variation reduces, making the laser output more suitable for applications. The first X-ray lasers [2] were produced using thin foil targets with complete ablation of the foils. It was soon found, however, that irradiation of thick slab targets with ablation of a thin layer of the target could produce lasing at 23 nm with relatively modest facilities [5]. Saturated X-ray laser output was observed for the first time with slab targets at 23 nm [6]. The next advance was to use a prepulse to create a preplasma with more gentle density gradients into which the main optical pumping pulse was incident [7], [8]. This increased the efficiency of the X-ray lasers mainly because with more gentle density gradients, the X-ray laser beam did not refract out of the gain volume in the plasma. Additionally, with prepulses it was found that the gain volume increased and the absorption of the main pumping pulse in the plasma increased. Pumping laser pulses of duration down to the picosecond have now been used to irradiate preplasmas created by prepulses with a resultant short duration of gain and output lasing duration [9], [10]. Recent work has shown that it is possible to have saturated X-ray lasing pumped with near table-top-sized picosecond duration optical lasers producing only a few joules of output [11].

Neon-like and nickel-like ions with closed shells of principal quantum number $n = 2$ and 3, respectively, have been observed to lase with collisional excitation pumping. The pumping mechanism was first proposed for neon-like ions in the 1970s [12], [13]. Lasing occurs between excited subshells $2p^5 3p \rightarrow 2p^5 3s$ (neon-like) or $3d^9 4d \rightarrow 3d^9 4p$ (nickel-like). The upper laser level in both iso-electronic series is metastable to decay to the ground state as the transition is electric dipole forbidden,

while the lower laser level can decay rapidly and directly to the ground state via the resonance dipole transitions $2p^5 3s \rightarrow 2p^6$ or $3d^9 4p \rightarrow 3d^{10}$. Lasing in the nickel-like ions has a higher quantum efficiency than for neon-like ions. Principally, because of the enhanced quantum efficiency, lasing at shorter wavelengths has been observed with nickel-like ions [3], [4]. The collisional excitation from the ground state to the upper laser level of the neon- and nickel-like ions occurs between two levels for which radiative dipole transitions are forbidden. However, the electron collisional excitation from the ground state to the upper lasing level occurs due to monopole excitation at a comparable rate to the collisional excitation for a strong electric dipole transition [14], [15].

Recent reviews on X-ray lasers should be referred to for more general information on the physics of X-ray lasers [16] or for reviews of different approaches to plasma-based X-ray lasing [17]–[19]. In this paper, recent experimental work on the development of X-ray lasers undertaken using the VULCAN laser at the Rutherford Appleton Laboratory is compared to detailed simulations. It is shown that short duration (~picosecond) pumping can produce X-ray laser pulses of a few picosecond duration and that measurement of the emission from the plasma can give an estimate of the duration of the gain coefficient. The Ehybrid fluid and atomic physics code developed at the University of York [20], [21] is used to simulate X-ray laser gain for comparison to our experiments. Two postprocessors to the Ehybrid code are utilized: 1) to raytrace the X-ray laser beam amplification and refraction and 2) to calculate the radiation emission in the kiloelectronvolt photon energy range [22]. The raytracing and spectral simulations are compared, respectively, to measured X-ray laser output and the output of diagnostics recording transverse X-ray emission, for example, a simple streak of the filtered emission. The pumping laser energy absorbed in the plasma is examined by comparing the simulations to experimental results. At high pumping irradiance ($> 10^{15}$ Wcm^{-2}), fast electrons are produced by parametric processes in the preformed long scalelength plasmas. These fast electrons do not pump the population inversion and so at high irradiance the pumping efficiency is reduced.

II. MEASUREMENTS OF SHORT WAVELENGTH PULSE DURATION

The measurement of the pulse duration of X-ray laser output is important for potential applications and to help understand gain and propagation conditions. The X-ray laser pulse duration defines the temporal resolution attainable in applications using X-ray lasers. The relationship between the gain duration and output laser pulse duration has been examined [23] using one-dimensional models following the work of Casperson [24] and Pert [25]. The model developed by Strati and Tallents [26] considers propagation of laser pulses along a length of gain medium with allowance for gain saturation and mismatches between traveling wave pumping and the X-ray pulse group velocity. It is clear that significant reduction of the X-ray laser pulse duration relative to the duration of gain is possible.

The measurement of X-ray laser pulses of picosecond duration is difficult as most X-ray streak cameras have temporal

resolution $>$3 ps [27]. Other possible techniques such as cross correlation with an optical beam are not yet proven [28]. It is desirable to spectrally resolve the X-ray laser line from possible long-lived broad-band background plasma emission using a spectrometer or multilayer mirror optic. However, spectrometer designs produce optical path length differences and hence temporal smearing. It is important to carefully minimize this temporal smearing in the operation of a spectrometer.

X-ray lasing was produced in Ni-like silver at 13.9 nm ($3p^6 3d^9 4d^1 S_0 \rightarrow 3p^6 3d^9 4p^1 P_1$) and Ne-like nickel at 23.1 nm ($3s^2 2p^5 3p^1 S_0 \rightarrow 3s^2 2p^5 3s^1 P_1$) by irradiating solid silver or nickel slabs with two beams of wavelength 1.06 μm from the VULCAN glass laser at the Rutherford Appleton Laboratory. For Ne-like nickel, a preplasma was formed with a background pulse of duration 280 ps and peak irradiance 2×10^{13} Wcm^{-2} in a line focus of length 16 mm and width 100 μm. The main pulse irradiance is enhanced by chirp pulse amplification (CPA) to give a duration of 1.2 ps and peak irradiance 7×10^{15} Wcm^{-2} in a line focus of length 12 mm and width 100 μm. To avoid overionizing the plasmas, the laser energy for Ni-like silver experiments was reduced to give irradiances of approximately 5×10^{12} Wcm^{-2} and 2×10^{15} Wcm^{-2} for the background and main pulse, respectively. The background pulse was produced from a component of the uncompressed main pulse and hence arrived on target without random jitter relative to the main pulse. The background pulse and main pulse were focused onto the targets with separate focusing systems comprising a refracting lens (the background pulse) or a parabolic shaped mirror (the main pulse) to produce a spot focus which was imaged in each case by an off-axis spherical mirror to produce the line focus on the target [29]. The experimental setup and results have been presented by Klisnick *et al.* [30] and Abou-Ali *et al.* [31].

The X-ray laser output was normally recorded using a flat field grating spectrometer [32] with an Axis Photonique streak camera positioned at the spectrometer detection plane. The flat field spectrometer was positioned so that the X-ray laser output was incident at a grazing angle of 3.55° onto a $n_g \approx 1200$ line/mm grating of radius of curvature 5.649 m. The spectrometer was operated at a distance of 420 mm from the end of the target. An aperture near the spectrometer grating defined the vertical angular acceptance (2.3 mrad) and ensured that only a length $d \approx 16$ mm of the grating in the direction along the grating surface normal to the grating rulings was illuminated. The distance d determines the temporal smearing Δt_g on the X-ray laser pulse produced by the grating. We have

$$\Delta t_g = \frac{d n_g \lambda}{c} \cong 0.9 \, \text{ps} \qquad (1)$$

where λ is the X-ray laser wavelength.

Raytracing shows that the aperiodic rulings on the grating [32] produce a planar focus at distance 237 mm from the grating. The grating was positioned horizontally so that the variation of the X-ray laser beam intensity with horizontal angle from the vertical target surface could be observed at the spectrometer detection plane. The spectrometer was initially operated with a charge-coupled device (CCD) detection system for each target material to check the position of the X-ray laser beam. The streak camera was subsequently positioned with a
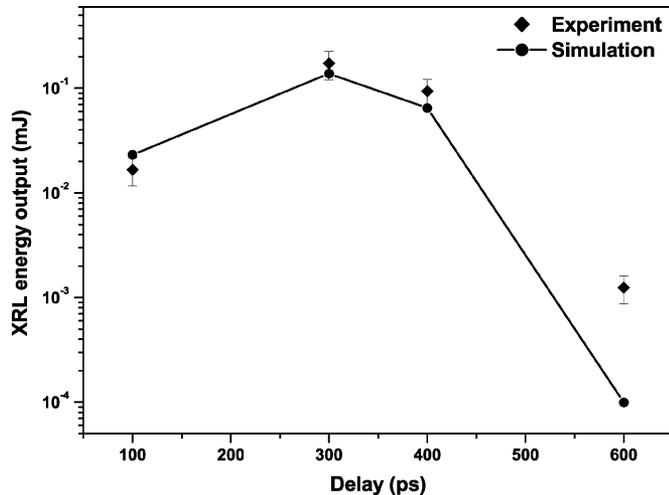
Fig. 1. Time-integrated energy output of the Ne-like Ni X-ray laser line at 23.1 nm from a target of length 4.3 mm as a function of the peak-to-peak separation between the CPA main 1.2-ps pulse and 280-ps background pulse.

vertical entrance aperture at the position of peak X-ray laser output recorded by the CCD camera. The peak-to-peak delay between the background and main pulse was varied to optimize the X-ray laser output using the flat field spectrometer with CCD detection (e.g., Fig. 1). For the Ne-like nickel and Ni-like silver results reported in this paper, we used a delay between pulses of 300 and 200 ps, respectively.

The streak camera was triggered using an Auston switch irradiated by a component of the chirped laser pulse separately compressed using a grating pair. This minimized jitter between the main laser pulse on target and the streak trigger. The streak camera was operated below saturation by using appropriate filters (e.g., $0.2 - 1.2$ μm plastic CH) to attenuate the X-ray beam so that space charge effects in the streak tube due to the production of too many photoelectrons did not degrade the temporal resolution. The streak camera temporal resolution and sweep speed were calibrated using frequency tripled pulses (wavelength 270 nm) from a 60-fs Ti:sapphiire laser operating at INRS, University of Quebec, Montreal [27]. With operation below saturation, the temporal resolution with a KI photocathode is estimated at 700 fs. Combining this resolution quadratically with Δt_g due to the spectrometer gives a total instrument temporal resolution of 1.1 ps. The streak camera sweep rate is $5(\pm 0.5)$ ps/mm.

The temporal variation of the Ni-like silver output at 13.9 nm and Ne-like nickel output at 23.1 nm as recorded with the streaked spectrometer is shown in Fig. 2. The X-ray laser outputs show a sharp rise with a slower fall in output in approximate agreement with both a geometric optics model [26] and geometric optics raytracing [22]. However, the experimental result shows a much greater level of oscillation than either the model or raytracing, even allowing for the high level of noise on the streak camera temporal profiles for timescales shorter than the temporal resolution (1.1 ps). The X-ray laser pulse duration [full-width at half-maximum (FWHM)] for silver was measured as $3.7(\pm 0.5)$ ps and for nickel as $10.7(\pm 0.5)$ ps, though there are shorter duration features in both temporal profiles. Interestingly, full raytracing does predict two peaks of
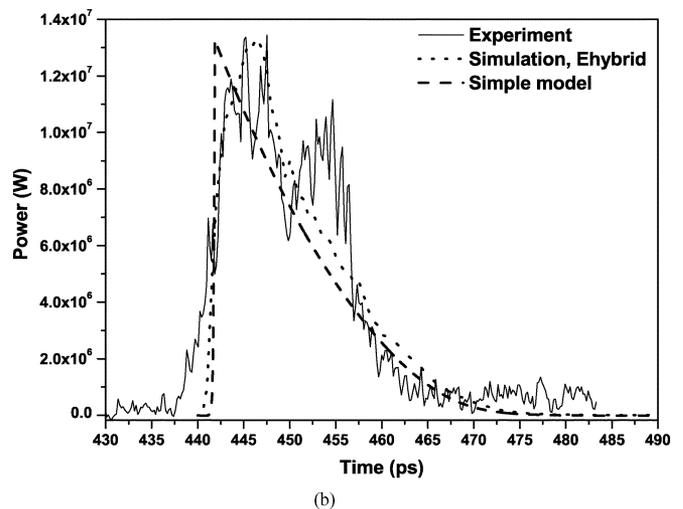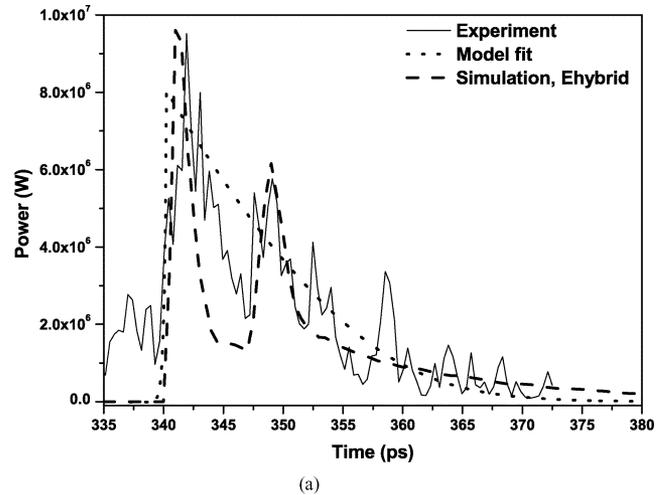

(a)

(b)

Fig. 2. Temporal variation of X-ray lasing at (a) 13.9 nm for Ni-like silver (10-mm target length) and (b) 23.1 nm for Ne-like nickel (6-mm target length). Intensity scales shown are arbitrary above the image intensifier and streak camera noise set at approximately zero level. Model fit for peak small signal gain of (a) 23 cm^{-1} or (b) 60 cm^{-1}, a gain duration of (a) 22 ps or (b) 35 ps and the ratio of spontaneous emission to the saturation irradiance $R = 10^{-6}$ (see [16]) is shown (as labeled). Fit obtained from three-dimensional ray traces [22] of the X-ray laser output is also superimposed (as labeled).

output in approximate agreement with experiment for Ni-like silver [see Fig. 2(a)].

The frequency range $\Delta\nu$ of the X-ray laser output is determined by thermal Doppler broadening of the gain profile and by gain narrowing. We may expect $\Delta\nu/\nu \sim 10^{-4}$ for Doppler broadening [25] and $\Delta\nu/\nu$ as small as 2×10^{-5} with gain narrowing [25], [26]. With the measured X-ray laser pulse output duration of $\Delta t = 3.7$ ps for Ni-like silver at 13.9 nm, this implies that the 13.9-nm X-ray laser pulses are close to Fourier transform limited with $\Delta\nu\Delta t \approx 1.5$.

III. ESTIMATION OF SHORT WAVELENGTH GAIN DURATION

The duration of gain is longer than the output laser-pulse duration [26]. However, measurement of the duration of gain in a plasma medium is difficult as the upper quantum states directly involved in the laser transition are metastable to decay to the ground state. If they were not metastable, the creation of a population inversion would not occur. Consequently, it is
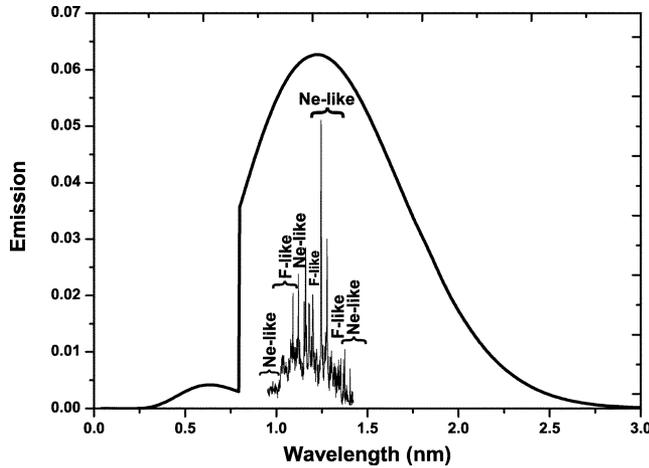
Fig. 3. Unfeatured curve shows on an arbitrary scale the relative bremsstrahlung emission of temperature 500 eV calculated to transmit through a 3.4-μm aluminum filter as used in the streaked slit diagnostic. Transmission is dominated by emission close in wavelength to the resonance lines of Ni-like silver and Ne-like nickel. Experimental spectrum on an arbitrary linear scale of nickel recorded using a crystal spectrometer, but modified to show the transmission through a 3.4-μm aluminum filter, is also superimposed to illustrate the detailed spectrum transmitted through the streaked slit diagnostic.

not possible to determine the laser upper quantum state population by directly measuring the resonance line emission from the upper state. We have shown that an estimate of the duration of the X-ray laser gain can be obtained by temporally resolving the spectrally integrated continuum and resonance line emission arising from states near in energy to the upper lasing level [22].

A simple streaked slit diagnostic was developed to record resonance line emission from states near in energy to the upper lasing levels. A Kentech streak camera with a thin gold photocathode (0.3 μm deposited on 1-μm aluminum) viewed the plasma transversely from the front side at an angle of 82.5° to the focal line. The estimated temporal resolution of $\approx$ 6 ps with this streak camera is dominated by the 500-μm-wide entrance slit. A space resolving slit of width 270 μm positioned normal to the timing slit gave spatial resolution $\approx$ 0.7 mm along the line focus length. A filter of 2.4-μm-thick aluminum (in addition to the 1-μm aluminum in the photocathode) was employed so that emission in the 0.8 – 2.1-nm wavelength range was recorded with the diagnostic (Fig. 3).

The emission recorded by the streaked slit diagnostic comprises continuum resonance lines of Ni-like silver (resonance emission in the range 1.7 to 2.2 nm from states with electron configurations $3p^63d^94p$, $3p^63d^94f$, $3p^53d^{10}4s$, and $3p^53d^{10}4d$) or Ne-like nickel (resonance emission in the range 1 to 1.4 nm from states with electron configurations $2s^22p^53s$, $2s^22p^53d$, and $2s2p^63p$) plus Co- or F-like lines, respectively (see e.g., Fig. 3). Using the model as fitted to Fig. 2, we have shown that the duration of emission recorded by the streaked slit diagnostic gives an estimate of the average gain coefficient duration in the plasma [31]. The reason for this is that the emission recorded by the streaked slit diagnostic peaks temporally and spatially in an approximately similar way to the gain coefficient. For example, for Ni-like silver, the gain and emission both peak at 20-μm distance from the target surface, while the gain peaks over times between 340 and 355 ps compared to
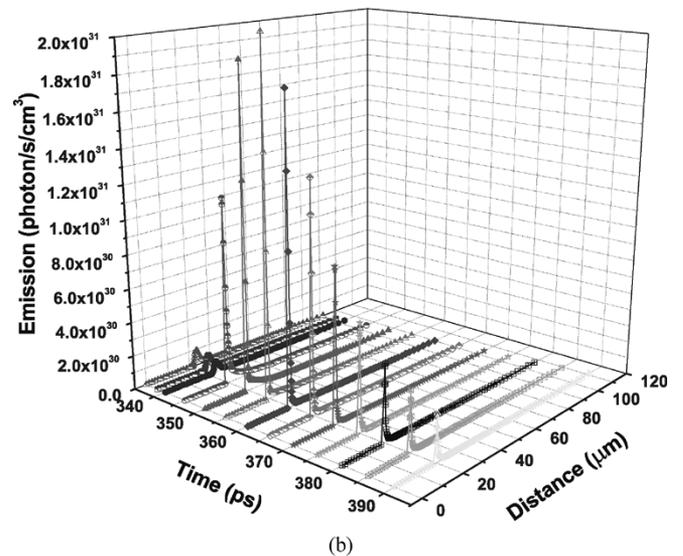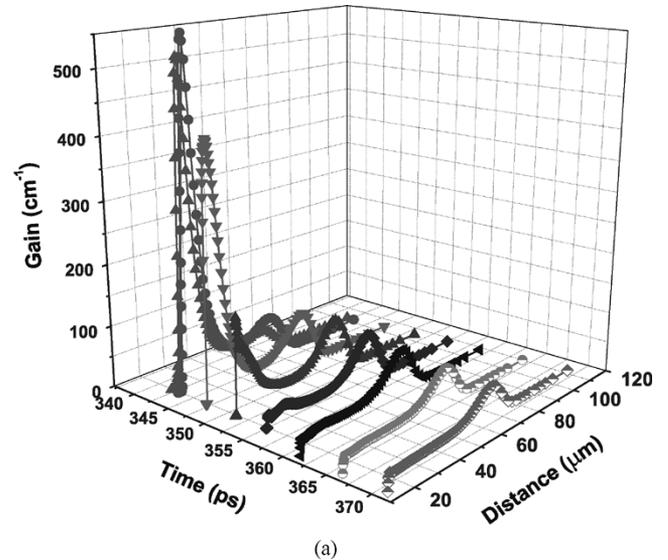

(a)

(b)

Fig. 4. (a) Gain coefficient for Ni-like silver lasing at 13.9 nm and (b) silver plasma emission as would be detected by the streaked slit camera as a function of distance from the target surface and time from the onset of the prepulse. Results are simulated using the EHYBRID fluid and atomic physics code.

the peak emission time between 335 and 365 ps (Fig. 4). For Ne-like nickel, the gain is over a wider spatial region from 15 – 100 μm and peaks temporally between 440–480 ps. The Ne-like nickel emission again peaks sharply at 20-μm distance from the target surface between 450–490 ps (Fig. 5). The times shown on Figs. 4 and 5 are the times from the onset of the prepulse and are different for Ni-like silver and Ne-like nickel because of the different time delays between the prepulses and main pulses.

The streaked slit output showing spatial resolution of 0.7 mm along the target length and temporal resolution of 6 ps is given in Fig. 6. Emission from the preplasma followed by the emission associated with the 1.2-ps main pulse is clearly apparent. Line-outs of emission associated with the short duration main pulse recorded by the streaked slit camera for the silver and nickel targets are shown in Fig. 7. There is a sharp rise in emission when the laser pulse is incident followed by an approximately exponential decrease with time. The emission associated with
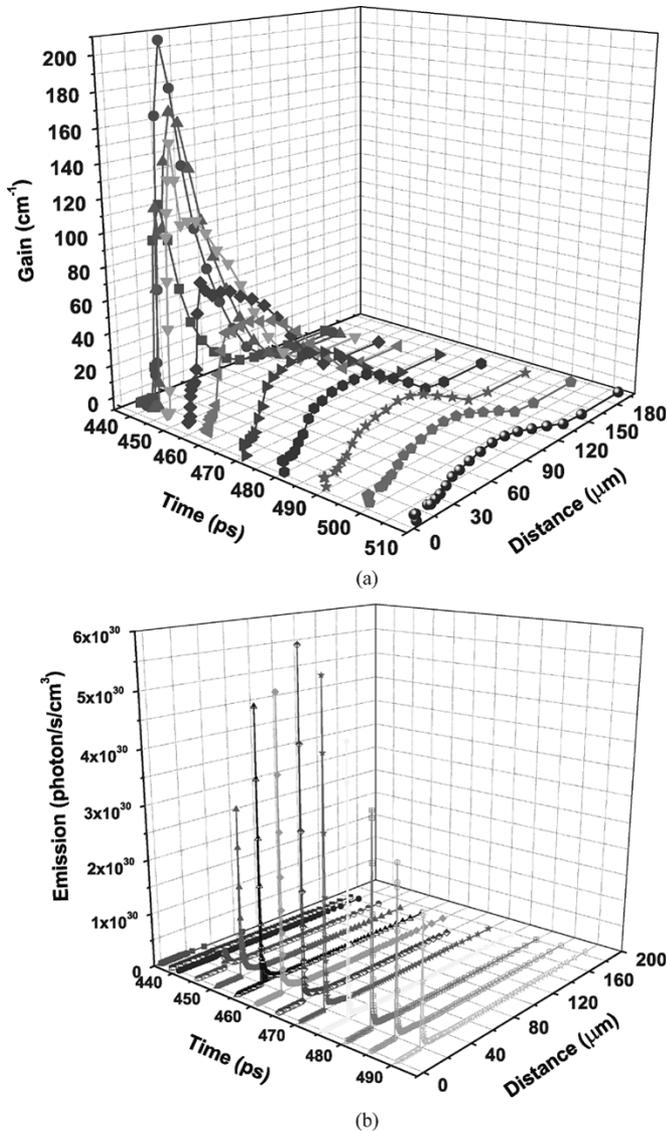
(a)

(b)

Fig. 5. (a) Gain coefficient of Ne-like nickel lasing at 23.1 nm and (b) nickel plasma emission as would be detected by the streaked slit camera as a function of distance from the target surface and time from the onset of the prepulse. Results are simulated using the EHYBRID fluid and atomic physics code.
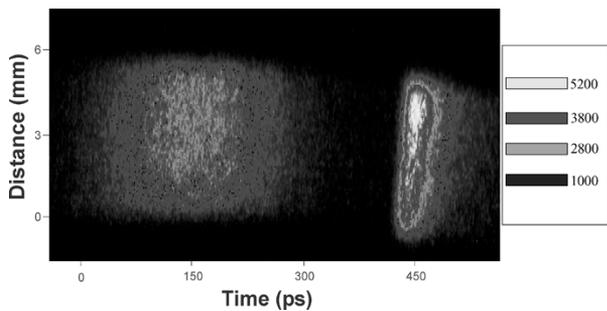

Fig. 6. Streaked slit camera image showing the plasma emission filtered by a 3.4-μm aluminum filter from the background and main laser pulses incident onto a nickel target. Relative intensity scale is also shown.

the short pulse laser has measured FWHM duration of 22($\pm$2) ps for silver and 35($\pm$3) ps for nickel targets. Simulations using the EHYBRID code of the radiation detected by the streaked
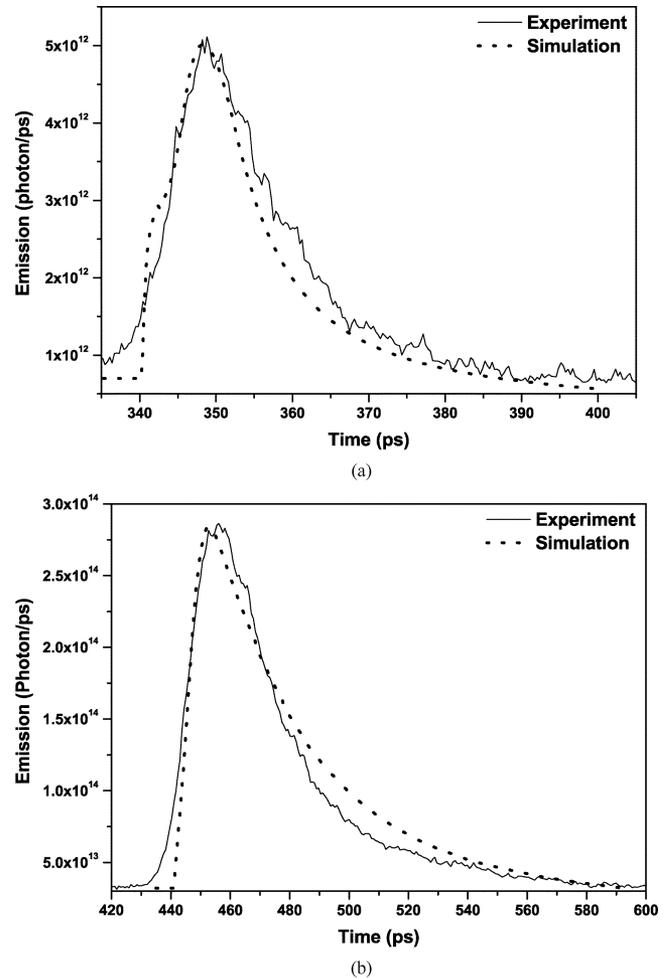

(a)

(b)

Fig. 7. Line-out of main pulse emission recorded by the streaked slit camera for (a) silver target and (b) nickel target. Simulation of the output obtained by postprocessing Ehybrid data is superimposed on the experimental measurements.

slit diagnostic fit the experimental time resolved emission (see Fig. 7).

IV. PUMPING LASER ABSORPTION

With picosecond pulse pumping of X-ray lasers, the irradiances on target are much greater (up to 10^{16} Wcm^{-2}) than used with experiments using higher energy longer pulse pumping lasers (typically up to 2×10^{14} Wcm^{-2}). In addition, the high irradiance pulses are incident into long scalelength plasmas due to the use of a prepulse, which means that parametric processes [33] may cause some of this absorbed energy to produce fast electrons that will not efficiently collisionally excite the population inversion. We have examined this indirect effect of parametric processes on the production of population inversions in X-ray laser experiments [34].

Simulations of X-ray laser experiments sometimes require a reduction of the assumed pump laser energy absorbed to obtain agreement with experiment [23], [35]. A correction factor $f \leq 1$ is utilized to multiply the actual incident laser energy to give a laser energy for use in the code simulations. We have determined the necessary value of f needed to model X-ray laser experiments involving picosecond duration pumping by comparing

the fluid and atomic physics code EHYBRID output with experimental results. To understand the cause of the reduced "effective energy" absorbed in the experiment, we model the laser energy absorption and resulting electron energy distribution using a particle-in-cell (PIC) code. The electron energy distribution calculated by the PIC code is used to calculate collisional excitation rates for comparison to the rates used in EHYBRID where Maxwellian distributions are used.

A PIC code [36], [37] simulated the 1-ps pulse interaction with a preformed plasma of profile and temperature as predicted by the EHYBRID code for the experimental conditions. An initial exponential density profile with an e^{-1} scalelength of 30 μm and temperature of 150 eV is used. For pumping laser irradiances greater than 10^{15} Wcm^{-2}, the PIC code shows the production of a two-temperature electron energy distribution (Fig. 8). The fraction of laser energy absorbed drops with increasing laser irradiance above 10^{15} Wcm^{-2} due to reduced inverse bremsstrahlung in the hotter plasmas at higher irradiance and the onset of parametric instabilities [34]. The electron phase-space distribution calculated by the PIC code indicates that the laser absorption at irradiances above 10^{15} Wcm^{-2} is due to inverse Bremsstralung and parametric instabilities around the region of the quarter critical density. These two processes produce the lower and higher temperature electron groups, respectively.

It is interesting to examine the effect of the two-temperature electron energy distribution on the monopole collisional excitation to the upper lasing level. For a specific electron energy distribution $f(v)$, the collisional excitation rate coefficient from the ground state to the upper lasing level of the Ne-like ion can be expressed as

$$K = \langle \sigma(v)v \rangle = \int_{\Delta E}^{\infty} \sigma(v)f(v)v dv \qquad (2)$$

where $\sigma(v) = \Omega/E$ is the collisional excitation cross section, Ω is the collision strength of the transition, while E and v are the energy and the velocity of electrons. ΔE is the excitation energy and, therefore, the threshold energy for the excitation of the upper lasing level. To investigate the effects of the two-temperature structure of the electron energy distribution from the PIC simulations, we compare the collisional excitation rate coefficient by the two groups of electrons from the PIC simulations with rates produced by electrons assuming a Maxwellian distribution with spatially averaged electron temperature (see [34]) as determined by the EHYBRID code.

The collision strength Ω for collisional excitation from the ground to the upper laser level is only weakly dependent on the exciting electron energy E so with good accuracy can be removed from within the integral of (2). Numerical results for $\langle \sigma(v)v \rangle / \Omega$ at the end of the 1-ps pulse are shown in Fig. 9 for neon-like germanium and nickel using the PIC code electron energy distribution and the EHYBRID determined Maxwellian distribution.

With the Maxwellian distribution used in the EHYBRID code, the calculated collisional excitation rates are higher than the values calculated with the two-temperature electron distribution calculated in the PIC code. An estimate of the f
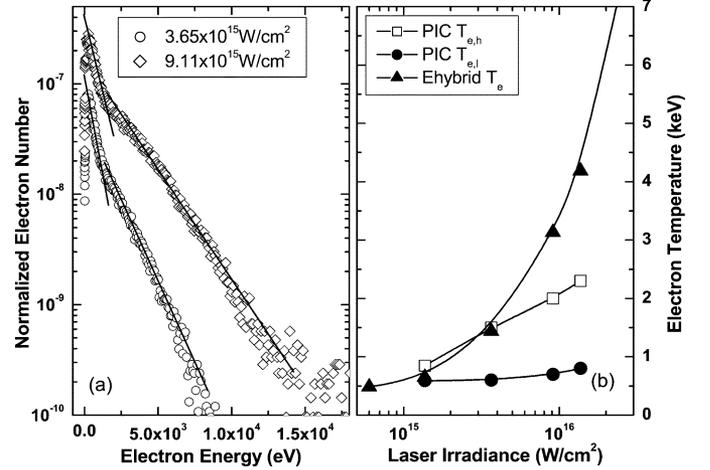

Fig. 8. (a) Electron energy distributions calculated by the PIC code showing the two-temperature structure for two different pumping laser irradiances. (b) Relation between pumping laser irradiance and the distance averaged temperature (solid up triangle) from the EHYBRID code and the lower (solid circle) and the higher temperature (hollow square) from PIC simulations.
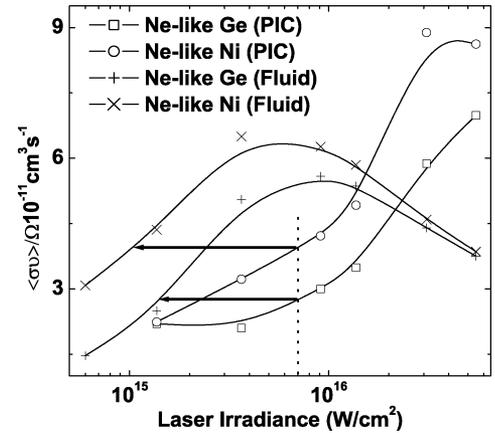

Fig. 9. Reduced collisional excitation rate coefficient of the upper lasing energy level for Ne-like Ni and Ge calculated assuming a Maxwellian electron distribution from the EHYBRID code and the electron distribution from PIC simulations at the end of the 1-ps pulse. Two arrows are shown joining the PIC and EHYBRID fluid code values of rate coefficient obtained for the experimental irradiance to illustrate the origin of the reduced irradiance needed for the fluid code simulations.

factor can be obtained from Fig. 9 by comparing $\langle \sigma v \rangle / \Omega$ from the PIC and EHYBRID codes. The ratio of irradiances required to produce comparable $\langle \sigma v \rangle / \Omega$ gives the value of f. It can be seen that an irradiance of 7×10^{15} Wcm^{-2} implies an f factor of 0.22 and 0.16 for Ne-like Ge and Ne-like Ni, respectively (see the arrows in Fig. 9).

To determine the correction factor f applicable for our experiment, a comparison of the simulated output of the EHYBRID code with different values of f and experimental results is made. The EHYBRID code models laser absorption by calculating the inverse bremsstrahlung absorption with a dump of 30% of energy reaching the critical density to allow for resonance and other absorption processes at critical. Laser energy not absorbed at the critical density is assumed to be reflected and the absorption by inverse bremsstrahlung as the light passes from the critical density to vacuum is evaluated. As inverse bremsstrahlung
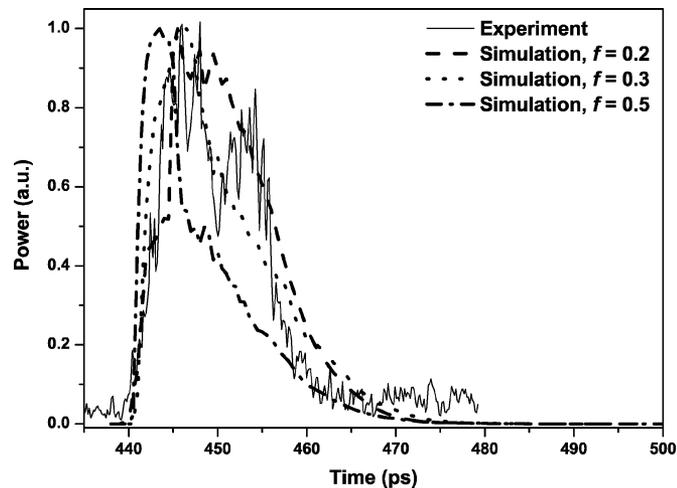
Fig. 10.   Simulated temporal variation of the Ne-like nickel X-ray laser output at 23.1 nm after raytracing for a target length of 6 mm superimposed on the experimental temporal variation of Ne-like nickel output recorded using a flat field spectrometer and a fast streak camera with different values of f (as labeled). Peak of the 1.2-ps pulse is incident at time 440 ps.

Fig. 11.   Simulated energy output of the Ne-like Ni X-ray laser at 23.1 nm after raytracing for a target of length 4.3 mm as a function of the peak-to-peak separation between the CPA main 1.2-ps pulse and 280-ps prepulse with correction factor $f = 0.2, 0.3,$ and 0.5 superimposed on the experimental time integrated energy output of the Ne-like Ni X-ray laser line at 23.1 nm recorded using a flat field spectrometer and CCD camera.

absorption dominates in the long scalelength plasmas, simulations show that the assumed dump at the critical density does not strongly affect the overall code-evaluated absorption.

The temporal variation of the Ne-like nickel output at 23.1 nm as recorded with the streaked spectrometer using an image intensifier is shown in Fig. 10. The simulated temporal variation of the Ne-like nickel X-ray laser output at 23.1 nm with different values of the correction factor f equal to 0.2, 0.3, and 0.5 are superimposed. The best agreement with the experiment is for $f = 0.2 - 0.3$.

A sequence of shots on 4.3-mm long Ni targets was taken to determine the optimum delay between the prepulse and the short pulse (Fig. 11). A relatively short target length was chosen to optimize the sensitivity of the measurement by avoiding both very small and very saturated signal strengths. The measurement of X-ray laser output assumes a grating efficiency of 1%, a CCD quantum efficiency at 23.1 nm of 0.47 photons per count, and the tabulated filter transmission of aluminum from Henke [38]. The total X-ray laser beam energy is determined by integration over solid angle assuming that the divergence of the X-ray laser in the vertical plane is twice that of the horizontal plane [22]. Fig. 11 also shows the Ne-like Ni X-ray laser energy output dependence on the arrival time of the peak of the main pulse relative to the peak of the prepulse from a numerical simulation with RAYTRACE postprocessing of the space-time output from the EHYBRID code superimposed. Different values of the correction factor f equal to 0.2, 0.3, and 0.5 have been used in the EHYBRID code. The best agreement has been obtained for $f = 0.3$ (Fig. 11).

Fig. 12 shows the simulated output of the Ne-like Ni X-ray laser with different values of f equal to 0.2, 0.3, and 0.5 superimposed on some single-shot experimental Ne-like Ni X-ray laser outputs. Good agreement between the simulations and the experimental points within the estimated experimental errors is obtained with $f = 0.3$ (Fig. 12). The error bars shown on the experimental points of Figs. 11 and 12 arise due to relative errors between the data points in integrating the output recorded
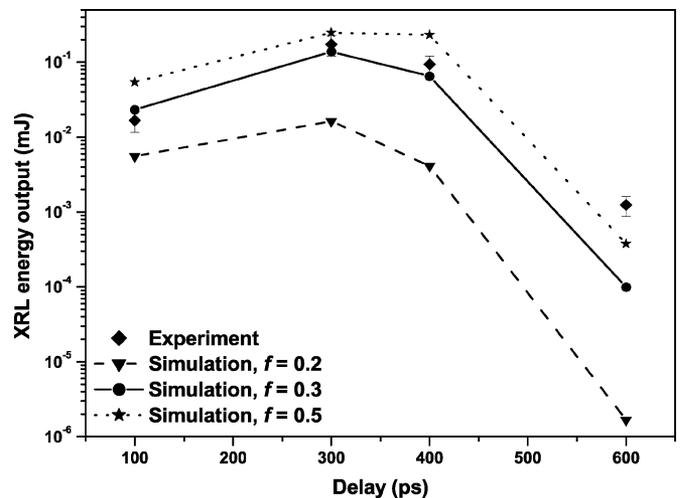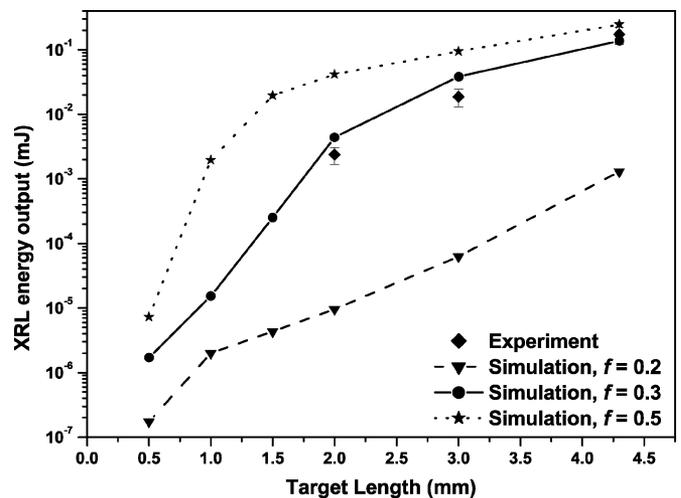

Fig. 12.   Ne-like Ni X-ray laser energy output from a numerical simulation with RAYTRACE postprocessing of the space-time output from the EHYBRID code as a function of target length with $f = 0.2, 0.3,$ and 0.5 superimposed on the experimental Ne-like Ni X-ray laser output recorded using a flat field spectrometer with CCD camera.

with the flat field spectrometer and the uncertainties of different filter thicknesses. The absolute magnitudes of the experimentally recorded X-ray laser outputs are also subject to an error (approximately a factor of two) that is not included in the error bars associated with the uncertainty in the reflectivity of the grating.

Spectrally integrated time-resolved experimental transverse emission emitted from a nickel plasma and recorded by the streaked slit diagnostic is shown in Fig. 13. The emission recorded by the streaked slit diagnostic comprises mainly continuum emission in the 0.6- to 1.8-nm spectral range and resonance lines of Ne-like nickel in the range of 0.95 to 1.45 nm plus F-like lines. Fig. 13 shows the simulated time-resolved transverse emission with different values of the correction factor f equal to 0.2, 0.3, and 0.5 superimposed. Though not
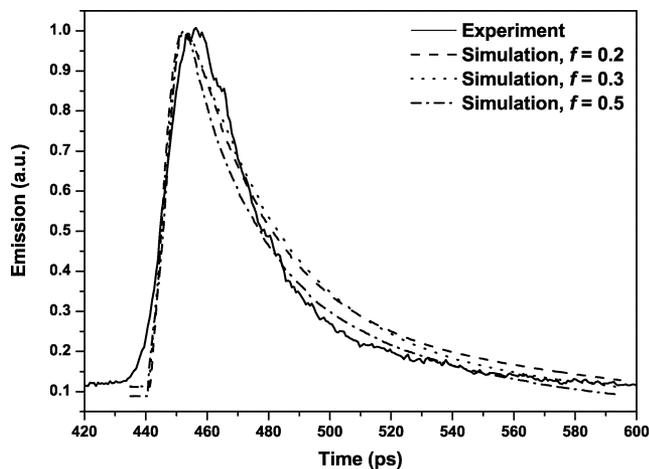
Fig. 13. Spectrally integrated time-resolved experimental and simulated transverse emission in the 0.6–1.8-nm spectral region emitted from a nickel plasma and recorded by a streaked slit diagnostic with different values of f (as labeled). Absolute emitted emission axis shown is taken from the simulation. Peak of the 1.2-ps pulse is incident at time 440 ps.

strongly dependent on the value of f, the best agreement of the simulated X-ray laser temporal profile with experiment is for $f = 0.3$ (Fig. 13).

V. CONCLUSION

Recent experimental work on the development of EUV lasers undertaken using as the pumping source the VULCAN laser at the Rutherford Appleton Laboratory has been compared to detailed simulations. It has been shown that short duration (~picosecond) pumping can produce X-ray laser pulses of a few picosecond duration and that measurement of the emission from the plasma can give an estimate of the duration of the gain coefficient. The Ehybrid fluid and atomic physics code developed at the University of York was used to simulate X-ray laser gain and plasma emission. The pumping laser energy absorbed in the plasma has been examined by comparing the simulations to experimental results. It has been shown that at high pumping irradiance ($> 10^{15}$ Wcm^{-2}) fast electrons are produced by parametric processes in the preformed long scalelength plasmas. These fast electrons do not pump the population inversion and so pumping efficiency is reduced at high irradiance.

REFERENCES

[1] R. W. Waynant and R. C. Elton, "Review of short wavelength laser research," *Proc. IEEE*, vol. 64, p. 1059, 1976.
[2] D. L. Matthews *et al.*, "Demonstration of a soft X-ray amplifier," *Phys. Rev. Lett.*, vol. 54, p. 110, 1985.
[3] B. J. MacGowan *et al.*, "Short wavelength X-ray laser research at the Lawrence Livermore National Laboratory," *Phys. Fluids*, vol. B4, p. 2326, 1992.
[4] R. Smith *et al.*, "Saturation behavior of two X-ray lasing transitions in Ni-like Dy," *Phys. Rev.*, vol. A59, p. R47, 1999.
[5] T. N. Lee, E. A. McLean, and R. C. Elton, "Soft X-ray lasing in neonlike germanium and copper plasmas," *Phys. Rev. Lett.*, vol. 59, p. 1185, 1987.
[6] A. Carillon *et al.*, "Saturated and near-diffraction-limited operation of an XUV laser at 23.6 nm," *Phys. Rev. Lett.*, vol. 68, p. 2917, 1992.
[7] J. Nilsen *et al.*, "Prepulse technique for producing low-Z Ne-like X-ray lasers," *Phys. Rev.*, vol. A48, p. 4682, 1993.
[8] H. Daido *et al.*, "Efficient soft X-ray lasing at 6 to 8 nm with nickel-like lanthanide ions," *Phys. Rev. Lett.*, vol. 75, p. 1074, 1995.
[9] P. V. Nickles, V. N. Shlyaptsev, M. Kalachnikov, M. Schnurer, I. Will, and W. Sander, "Short pulse X-ray laser at 32.6 nm based on transient gain in Ne-like titanium," *Phys. Rev. Lett.*, vol. 78, p. 2748, 1997.
[10] J. Y. Lin *et al.*, "Travelling wave chirped pulse amplified transient pumping for collisional excitation lasers," *Opt. Commun.*, vol. 166, p. 211, 1999.
[11] J. Dunn, A. L. Osterheld, J. Nilsen, J. R. Hunter, and V. N. Shlyaptsev, "Gain saturation regime for laser-driven tabletop transient Ni-like ion X-ray lasers," *Phys. Rev. Lett.*, vol. 84, p. 4834, 2000.
[12] R. C. Elton, "Extension of 3p$- > $3s ion lasers into the vacuum ultraviolet region," *Appl. Opt.*, vol. 14, p. 97, 1975.
[13] A. V. Vinogradov, I. I. Sobelman, and E. A. Yukov, "Feasibility of a far ultraviolet laser utilizing transitions of mulicharged ion in inhomogeneous plasma," *Kvantovaya Elektronika*, vol. 2, p. 105, 1975.
[14] P. L. Hagelstein, "Relativistic distorted-wave results for nickel-like gadolinium," *Phys. Rev.*, vol. A34, p. 874, 1986.
[15] H. Daido *et al.*, "Atomic number scaling of the nickel-like soft X-ray lasers," *Int. J. Mod. Phys.*, vol. B11, p. 945, 1997.
[16] G. J. Tallents, "The physics of soft X-ray lasers pumped by electron collisions in laser-plasmas," *J. Phys.*, vol. D36, p. R259, 2003.
[17] J. J. Rocca, "Table-top soft X-ray lasers," *Rev. Sci. Instrum.*, vol. 70, p. 3799, 1999.
[18] H. Daido, "Review of soft X-ray laser researches and developments," *Rep. Prog. Phys.*, vol. 65, p. 1513, 2002.
[19] D. Attwood, *Soft X-rays and Extreme Ultra-Violet Radiation: Principles and Applications*. Cambridge, U.K.: Cambridge Univ. Press, 1999, ch. 7.
[20] G. J. Pert, "The hybrid model and its application for studying free expansion," *J. Fluid Mech.*, vol. 131, p. 401, 1983.
[21] P. B. Holden *et al.*, "A computational investigation of the neon-like germanium collisionally pumped laser," *J. Phys.*, vol. B27, p. 341, 1994.
[22] Y. Abou-Ali, A. Demir, G. J. Tallents, M. Edwards, R. E. King, and G. J. Pert, "Comparison of simulated and experimental time resolved emission for a Ne-like nickel X-ray laser," *J. Phys.*, vol. B36, p. 4097, 2003.
[23] R. E. King *et al.*, "Saturated X-ray lasers at 196 and 73 Å pumped by a picosecond travelling wave excitation," *Phys. Rev.*, vol. A64, p. 053 810, 2001.
[24] L. Casperson and A. Yariv, "Pulse propagation in a high-gain medium," *Phys. Rev. Lett.*, vol. 26, p. 293, 1971.
[25] G. J. Pert, "Output characteristics of amplified-stimulated-emission lasers," *J. Opt. Soc. Amer.*, vol. B11, p. 1425, 1994.
[26] F. Strati and G. J. Tallents, "Analytical modeling of group-velocity effects in saturated soft-X-ray lasers pumped with a picosecond travelling wave excitation," *Phys. Rev.*, vol. A64, p. 013 807, 2001.
[27] P. Gallant *et al.*, "Characterization of a subpicosecond X-ray streak camera for ultrashort laser-produced plasmas experiments," *Rev. Sci. Instrum.*, vol. 71, p. 3627, 2000.
[28] E. Constant, E. Mevel, A. Zair, V. Bagnoud, and F. Salin, "Toward sub-femtosecond pump-probe experiments: A dispersionless autocorrelator with attosecond resolution," *J Phys. IV*, vol. 11, no. Pr 2, p. 537, 2000.
[29] I. N. Ross, "Design and performance of a new line focus geometry for X-ray laser experiments," *Appl. Opt.*, vol. 36, p. 9348, 1997.
[30] A. Klisnick *et al.*, "Demonstration of a 2 ps transient X-ray lasers," *Phys. Rev.*, vol. A65, p. 033 810, 2002.
[31] Y. Abou-Ali, G. J. Tallents, M. Edwards, R. E. King, G. J. Pert, S. J. Pestehe, F. Strati, R. Keenan, C. L. S. Lewis, S. Topping, O. Guilbaud, A. Klisnick, D. Ros, R. Clarke, D. Neely, M. Notley, and A. Demir, "Measurement of the duration of X-ray lasing pumped by an optical laser pulse of picosecond duration," *Opt. Commun.*, vol. 215, p. 397, 2003.
[32] T. Kita, T. Harada, N. Nakano, and H. Kuroda, "Mechanically ruled aberration-corrected concave gratings for a flat-field grazing-incidence spectrograph," *Appl. Opt.*, vol. 22, p. 512, 1983.
[33] H. A. Baldis, E. M. Campbell, and W. L. Kruer, *Handbook of Plasma Physics*, M. N. Rosenbluth and R. Z. Sagdeev, Eds. Amsterdam, The Netherlands: Elsevier, 1991, p. 361.
[34] Y. Abou-Ali, Q. L. Dong, A. Demir, R. E. King, G. J. Pert, and G. J. Tallents, "Quantitative simulations of short pulse X-ray laser experiments," *J. Phys. B*, vol. 37, pp. 2855–2868, 2004.

[35] G. F. Cairns, S. B. Healy, C. L. S. Lewis, G. J. Pert, and E. Robertson, "A time-resolved spectroscopy study of the resonance-line emission in the Ge XXIII XUV laser," *J. Phys. B*, vol. 29, pp. 4839–4854, 1996.

[36] Z. M. Sheng, Y. Sentoku, K. Mima, J. Zhang, W. Yu, and J. Meyer-ter-Vehn, "Angular distributions of fast electrons, ions, and bremsstrahlung γ-Rays in intense laser interaction with solid targets," *Phys. Rev. Lett.*, vol. 85, pp. 5340–5343, 2000.

[37] Q. L. Dong, Z. M. Sheng, M. Y. Yu, and J. Zhang, "Optimization of ion acceleration in the interaction of intense femtosecond laser pulses with ultrathin foils," *Phys. Rev. E*, vol. 68, p. 026408, 2003.

[38] B. L. Henke, E. M. Gullikson, and J. C. Davis, "X-ray interactions: Photoabsorption, scattering, transmission, and reflection at $\mathrm{E} = 50 - 30,000$ eV, $Z = 1 - 92$," *At. Data Nucl. Data Tables*, vol. 54, p. 181, 1993.

G. J. Tallents, photograph and biography not available at the time of publication.

Y. Abou-Ali, photograph and biography not available at the time of publication.

A. Demir, photograph and biography not available at the time of publication.

Q. Dong, photograph and biography not available at the time of publication.

M. H. Edwards, photograph and biography not available at the time of publication.

P. Mistry, photograph and biography not available at the time of publication.

G. J. Pert, photograph and biography not available at the time of publication.